

# RECONSTRUCTION OF IMAGES WITH FINITE RATE OF INNOVATION FROM NOISY TOMOGRAPHIC PROJECTIONS

Renke Wang<sup>\*</sup>, Thierry Blu<sup>†</sup>, Pier Luigi Dragotti<sup>\*</sup>

<sup>\*</sup>Imperial College London

<sup>†</sup>The Chinese University of Hong Kong

email: renke.wang19@imperial.ac.uk, thierry.blu@m4x.org, p.dragotti@imperial.ac.uk

**Abstract**—In this paper, we propose a robust 2D tomographic reconstruction algorithm for classes of piecewise constant images whose edges are defined by curves with finite rate innovation (FRI). The curve is known to satisfy an annihilation relation associated with the derivative of the image. Given limited numbers of noisy projections and inaccurately known angles, unlike conventional methods that are directly reconstructing images from projections, we first recover the curve exploiting the frequency domain annihilation relation. Once the curve is retrieved, we leverage the spatial domain interpretation of the annihilation relation, and formulate the image reconstruction as a regularized optimization problem. To enhance the reconstruction quality, we further refine the angles given the reconstructed image and iterate the process. Experiments show that by doing so, we can robustly reconstruct the 2D image even from limited numbers of severely corrupted projections and highly inaccurate projection angles.

**Index Terms**—2D tomographic reconstruction, annihilable curve, finite rate of innovation, angle refinement

## I. INTRODUCTION

The problem of reconstructing an unknown 2D or 3D structure from a set of tomographic projections has gained huge prominence as it applies to multitude of imaging problems. Examples of such include medical imaging [1], [2], cryogenic electron microscopy (cryo-EM) [3]–[5] and industrial radiography [6], to name a few. It is often assumed that the projection angles are known in advance. Yet there are instances when these angles are only known approximately. Take computed tomography (CT) as an example, the projection angles are supposed to be known a-priori through the acquisition process. However, due to unknown patient motion and measurement uncertainty, the angles are only approximately known [7]. The projections are normally heavily corrupted by noise, which again results in inaccurate angle estimation [8], [9]. In this paper, we focus on 2D tomographic reconstruction problem under the above mentioned settings and assume a limited numbers of noisy projections and inaccurately known projection angles.

The tomographic inversion problem with known angles is typically treated as a linear inverse problem. Conventional methods such as filtered back projection (FBP) and direct Fourier methods [10], [11] make use of central slice theorem. They work adequately when the projections are relatively clean and exact knowledge of the projection angles is available. Other methods formulate a regularized optimization problem to reconstruct the image by imposing prior knowledge of the image [12]–[17], such as smoothness or sparsity. Yet the

performance is limited by the number of available projections. In both known and unknown angle tomographic reconstruction, angle refinement based on projection matching is widely applied to enhance the reconstruction performance [1], [17].

We notice that one intrinsic limitation of applying the central slice theorem to the tomographic reconstruction problem is that the 1D Fourier measurements fill the 2D plane radially which results in high concentration of low frequency measurements and sparse high frequency measurements. This intrinsic limitation makes most reconstruction algorithms data demanding. In this paper, we consider piecewise constant images defined by curves with finite rate of innovation [18]. Instead of directly reconstructing the image from projections, we first retrieve the image curves using a robust FRI reconstruction algorithm [19]. The image is then recovered based on using the spatial domain annihilation relation for a regularized optimization problem. Finally, to enhance the performance, we introduce a method to refine the projection angles based on the previously reconstructed 2D image.

The rest of the paper is organized as follows: we provide the problem formulation in Sect. II and explain our reconstruction method in Sect. III. Then, we validate the proposed method with experiments done with synthetic data in Sect. IV. We conclude the paper in Sect. V.

## II. PROBLEM DESCRIPTION

### A. FRI Curve and Image Model

We consider a specific class of curves  $C$  defined by the zero-level set of a bandlimited periodic trigonometric polynomial  $\mu(x, y)$  [18]:

$$C = \{x \in [0, \tau_x], y \in [0, \tau_y] : \underbrace{\sum_{k=-K_0}^{K_0} \sum_{l=-L_0}^{L_0} c_{k,l} e^{j \frac{2\pi k x}{\tau_x} + j \frac{2\pi l y}{\tau_y}}}_{\mu(x,y)} = 0\}, \quad (1)$$

where  $K_0, L_0 \in \mathbb{Z}^+$ , and  $c_{k,l} \in \mathbb{C}$  are coefficients of the complex exponentials. We define the degree of polynomial  $\mu(x, y)$  to be the size of the smallest rectangle that contains the frequency support of  $\mu$ , and it equals the rate of innovation of the curve  $C$ :  $\deg(\mu) = \rho(C) = (2K_0 + 1, 2L_0 + 1)$ . Moreover, we enforce the polynomial to be real-valued so that  $\mu(x, y) = 0$  has always curves as solutions, as shown in Fig. 1 (a), which is equivalent to saying that the coefficients are Hermitian symmetric  $c_{k,l} = c_{-k,-l}^*$ .

It has been proven [18] that for this class of curves defined in Eq. (1), there exists a continuous domain piecewise constant image  $I(x, y)$ , such that the Fourier transform of the Wirtinger derivative of the image  $\hat{I}(\omega_x, \omega_y)$  is annihilated by convolving it with a filter made of the coefficients  $c_{k,l}$  of the bandlimited trigonometric polynomial, as shown in Fig. 1. (d). Specifically, we define the image model  $I(x, y)$  as follows:

$$I(x, y) = 1_{U_C}(x, y), \quad \forall (x, y) \in [0, \tau_x] \times [0, \tau_y], \quad (2)$$

where  $U_C \subset [0, \tau_x] \times [0, \tau_y]$  is a region with boundaries defined by the curve  $C$  as shown in Fig. 1 (b). Here  $U_C = \{(x, y) : \mu(x, y) \geq 0\}$ , and  $1_{U_C}$  denotes the plane indicator function:

$$1_{U_C} = \begin{cases} 1, & \text{for } (x, y) \in U_C, \\ 0, & \text{otherwise.} \end{cases}$$

The Wirtinger derivative of the image  $I'(x, y) = \partial_x I(x, y) + j\partial_y I(x, y)$  behaves like Dirac  $\delta$  along the curve  $C$ . Therefore, since  $\mu(x, y)$  is zero on the curve  $C$ , we have that:

$$\mu(x, y)I'(x, y) = 0. \quad (3)$$

This is shown in Fig. 1 (c). In frequency domain, the annihilation property is a convolution between the coefficients  $c_{k,l}$  and the uniform discrete Fourier measurements of the image  $\hat{I}(\omega_x, \omega_y)$ :

$$\sum_{k=-K_0}^{K_0} \sum_{l=-L_0}^{L_0} c_{k,l} \hat{I}\left(\omega_x - \frac{2\pi k}{\tau_x}, \omega_y - \frac{2\pi l}{\tau_y}\right) = 0. \quad (4)$$

### B. Projection acquisition

We consider a set of  $N$  tomographic projections  $\{g_i(t)\}_{i=1}^N$  of the 2D image taken at angles  $\{\theta_i\}_{i=1}^N$ :

$$g_i(t) = \int_0^{\tau_y} \int_0^{\tau_x} I(x, y) \delta(x \cos \theta_i + y \sin \theta_i - t) dx dy,$$

where  $\delta(\cdot)$  is the Dirac distribution. We consider the challenging setting where the projections  $\tilde{g}_i(t)$  are corrupted with strong noise and the initial angles  $\{\theta_i\}_{i=1}^N$  deviate from the true values:

$$\begin{aligned} \tilde{\theta}_i &= \theta_i + \beta_i, \\ \tilde{g}_i(t) &= g_i(t) + \epsilon_i(t), \end{aligned}$$

where  $\epsilon_i(t)$  is additive Gaussian white noise with zero mean and variance  $\sigma_\epsilon^2$ , and  $\{\beta_i\}_{i=1}^N$  are zero mean uniformly distributed random variable in  $[-\epsilon_\theta, \epsilon_\theta]$  rad.

## III. RECONSTRUCTION METHOD

### A. Curve recovery from inaccurate non-uniform Fourier measurements

Central slice theorem states that the Fourier transform of the 1D projection at angle  $\theta_i$  is equal to the Fourier transform of its corresponding 2D image sliced through the origin in the parallel direction to the projection line:

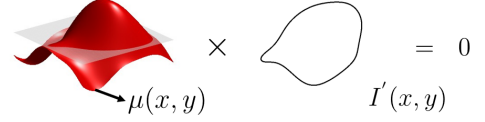
$$\mathcal{F}_{1D}\{g_i(t)\}(\omega) = \mathcal{F}_{2D}\{I(x, y)\}(\omega \cos \theta_i, \omega \sin \theta_i).$$



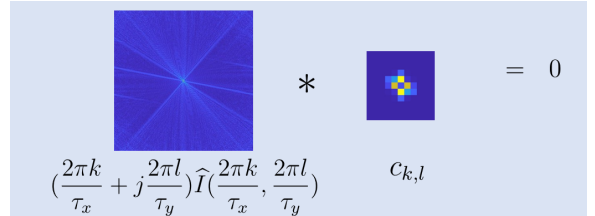
(a) The curve  $C$  is the zero level set of the trigonometric polynomial  $\mu(x, y)$ .



(b) Piecewise constant image  $I(x, y)$  defined by curve  $C$ .



(c) Spatial domain interpretation of the annihilation relation.



(d) Frequency domain interpretation of the annihilation relation.

Fig. 1: Signal model.

Therefore, given noisy projections and inaccurately known projection angles, we can obtain a set of Fourier measurements  $\{\hat{I}(\omega \cos \tilde{\theta}_i, \omega \sin \tilde{\theta}_i)\}_{i=1}^N$ . We stack all these measurements in a vector denoted with  $\mathbf{a}$ . Clearly, these measurements are non-uniformly taken in the frequency plane. The conventional reconstruction approach in the field of finite rate of innovation is to look for a discrete filter such that its convolution with the uniform Fourier samples of the image is zero, as stated in Eq. (4). Therefore, the question is whether we can recover the curve coefficients  $\mathbf{c} : \{c_{k,l}\}$  robustly from these non-uniform noisy Fourier measurements  $\mathbf{a}$ .

The reconstruction problem can be reformulated as an approximation problem by fitting an FRI model that is consistent with the measurements. The FRI curve model requires the annihilation constraint to be satisfied. At the same time, after reconstructing the FRI signal, if we re-synthesize the measurements, they have to be consistent with the given measurements. We adopt a constrained approximation formulation to this problem as proposed in [19]:

$$\begin{aligned} &\text{find } \mathbf{b}, \mathbf{c} \in \mathcal{C} \\ &\text{subject to } (\mathbf{R}(\mathbf{c}) \odot \mathbf{s})\mathbf{b} = \mathbf{0}, \\ &\quad \|\mathbf{a} - \mathbf{G}\mathbf{b}\|_2^2 \leq \sigma_\epsilon^2, \end{aligned}$$

where

- $\mathbf{a}$  is the vector of non uniform Fourier measurements obtained from the projections;
- $\mathbf{b}$  is the vector of discrete uniform Fourier measurements that satisfies the annihilation constraint;

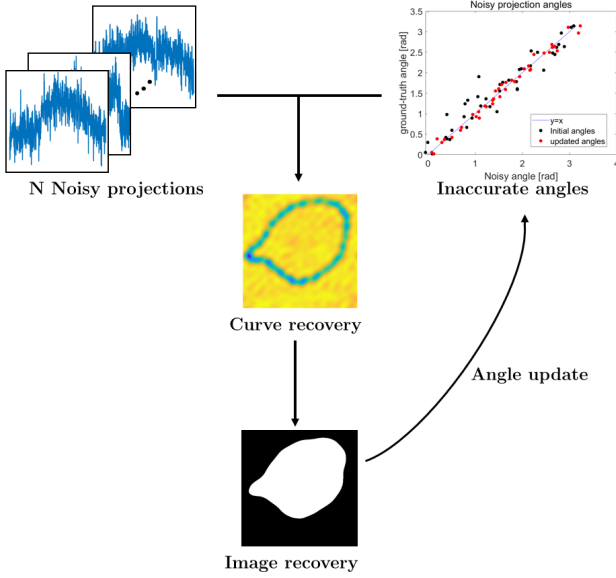


Fig. 2: Overall scheme for the proposed method.

- $\mathbf{c}$  is the curve coefficients that annihilates  $\mathbf{b}$ ,  $\mathbf{R}(\cdot)$  is the Toeplitz structured convolution matrix;
- $\mathbf{s}$  is the frequency scaling factor  $(\frac{2\pi k}{\tau_x} + j\frac{2\pi l}{\tau_y})$  associated with the annihilation relation, and  $\odot$  denotes the Hadamard product;
- $\mathbf{G}$  denotes the linear mapping between the measurements  $\mathbf{a}$  and the uniform measurements  $\mathbf{b}$  (uniform interpolation). In our case, it represents a 2D sinc kernel, because our image is support limited.

The constrained approximation can be solved using an iterative scheme proposed in [19]. Note that if the annihilation matrix  $\mathbf{R}(\mathbf{c}) \odot \mathbf{s}$  is built with the correct filter support, i.e.  $\deg(\mu) = \rho(C)$ , the null space (a.k.a annihilating subspace) is one-dimensional, from which coefficients  $\mathbf{c}$  can be retrieved using the annihilation relation. In cases when the correct filter support is unknown and the given measurements are very noisy, we can assume a filter support strictly larger than the correct one, i.e.  $\deg(\mu) > \rho(C)$ . In this case, the annihilating subspace will have dimension larger than 1. In this work, we leverage this redundancy to retrieve several polynomials  $\mu_n(x, y)$ . Each  $\mu_n$  can be written in the form  $\mu_n = \eta_n \mu$ , where  $\eta_n$  is another trigonometric polynomial. Therefore, the desired curve is the common zeros of the set of polynomials  $\mu_n$  and can be retrieved as the sum of squares (SoS):

$$\bar{\mu}(x, y) = \sqrt{\sum_{n=1}^N |\mu_n(x, y)|^2}. \quad (5)$$

### B. Image recovery based on spatial formulation of the annihilation constraint

Once the polynomial  $\bar{\mu}(x, y)$  is retrieved, we can estimate the image based on the spatial domain interpretation of the annihilation relation as stated in Eq. (3). The objective function we want to minimize is:

---

### Algorithm 1 Primal-dual algorithm

---

**Require:** step size  $\tau_1, \tau_2 > 0$ ,  $\lambda_1, \lambda_2$

- 1:  $k = 0$ , pick  $I^0$  and a feasible  $\mathbf{v}^0$
  - 2: **for**  $k \leq K$  **do**
  - 3:  $\mathbf{v}^{k+1} = \mathbf{P}_{\|\mathbf{v}\| \leq 1}(\mathbf{v}^k + \tau_1 \mathcal{W} I^k)$
  - 4:  $\mathbf{h} = I^k - \tau_2 \mathcal{W}^T \mathbf{v}^{k+1} + \tau_2 \lambda_1 \mathcal{A}^T \mathbf{b}$
  - 5:  $I^{k+1} = \mathbf{h} / (1 + \tau_2 \lambda_1 \mathcal{A}^T \mathcal{A} + \tau_2 \lambda_2 \Delta^T \Delta)$
  - 6: **end for**
- 

$$\min_I \|\bar{\mu} \odot I'\|_{1,1} + \lambda_1 \|\mathcal{A}I - \mathbf{b}\|_2^2 + \lambda_2 \|\Delta I\|_2^2,$$

where  $I$  is the reconstructed image,  $I'$  is approximated using finite differences and the first term imposes the annihilation constraint.  $\mathcal{A}$  and  $\Delta$  are the DFT operator and discrete Laplacian operator, and they are used to impose data consistency and image smoothness. The above weighted total variation minimization problem can be re-written in a min-max formulation:

$$\min_I \max_{\|\mathbf{v}\| \leq 1} \Phi(I, \mathbf{v}) := (\mathcal{W}I)^T \mathbf{v} + \lambda_1 \|\mathcal{A}I - \mathbf{b}\|_2^2 + \lambda_2 \|\Delta I\|_2^2,$$

where  $\mathcal{W}$  is a linear operator that computes the weighted finite differences. The min-max problem can then be solved through iterative primal-dual approach [20]. In  $k$ th iteration, at the dual step we apply one step of gradient descent to update the auxiliary variable  $\mathbf{v}^k$  with  $I^k$  fixed, while at the primal step, we update  $I^k$  with  $\mathbf{v}^{k+1}$  fixed. The updating steps are summarized in **Algorithm 1**.

---

### Algorithm 2 Angle updating algorithm

---

**Require:**  $\tau > 0, \gamma \in (0, 1), \delta, \theta^0 = \bar{\theta}, \bar{\mathbf{g}}, k = 0, K$

- 1: **for**  $k \leq K$  **do**
  - 2:  $\tau \leftarrow \tau^0$ ,  $\text{flag} \leftarrow 1$ ,  $\zeta \leftarrow \theta^k$
  - 3: **while**  $\text{flag}$  **do**
  - 4:  $\zeta_i^{tmp} = \zeta_i - \tau \nabla \mathcal{J}(\zeta_i)$
  - 5: update  $\theta_i^{k+1}$  if  $(\mathcal{J}(\zeta_i^{tmp}) \leq \mathcal{J}(\zeta_i))$
  - 6: exclude updated angles from  $\zeta$
  - 7:  $\text{flag} \leftarrow 0$  if  $\text{len}(\zeta) == 0$
  - 8:  $\tau = \tau * \gamma$
  - 9: **end while**
  - 10: **end for**
- 

### C. Angle refinement based on the reconstructed image

Given the first estimation of the image, we then refine the projection angles based on the previously reconstructed image. This can be done using approximate gradient descent method. Specifically, we set the measured projections  $\bar{\mathbf{g}} : \{\bar{g}_i(t)\}_{i=1}^N$  as reference, and use  $\mathbf{g}(\gamma) : \{g_{\gamma_i}(t)\}_{i=1}^N$  to represent re-synthesized projections from the reconstructed image at angles  $\gamma : \{\gamma_i\}_{i=1}^N$ . We define the cost function at angles  $\gamma_i$  as  $\mathcal{J}(\gamma_i) = \|\bar{g}_i - g_{\gamma_i}\|_2^2$ . The approximate gradient at angles  $\gamma_i$  is defined as  $\nabla \mathcal{J}(\gamma_i) = \frac{\mathcal{J}(\gamma_i + \delta) - \mathcal{J}(\gamma_i)}{\delta}$ , where  $\delta$  is a small enough angle. In each iteration, we operate by updating the

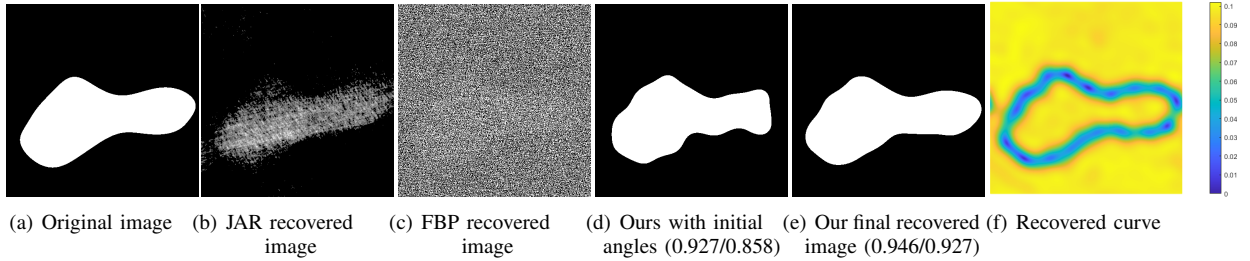


Fig. 3: Visual comparison of reconstructed images by our proposed method, JAR method and FBP method. Compared to the original image, the SSIM and IoU of our reconstructed image are 0.946 and 0.927 respectively (40 projection angles with  $\epsilon_\theta = 0.5$  rad, projection SNR = 5dB).

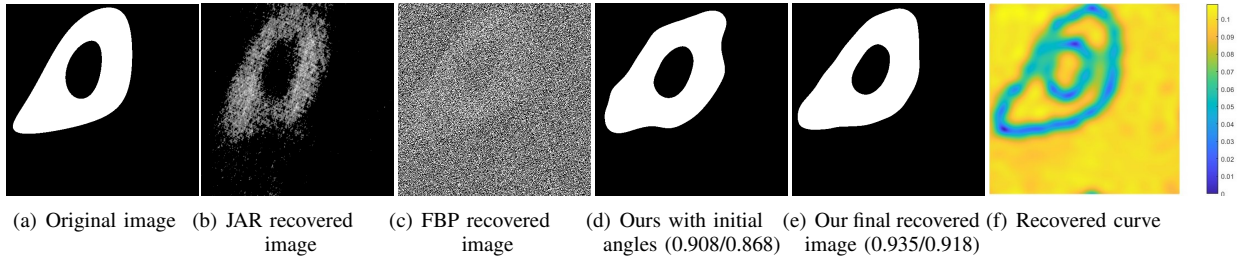


Fig. 4: Visual comparison of reconstructed images by our proposed method, JAR method and FBP method. Compared to the original image, the SSIM and IoU of our reconstructed image are 0.935 and 0.918 respectively (40 projection angles with  $\epsilon_\theta = 0.5$  rad, projection SNR = 5dB).

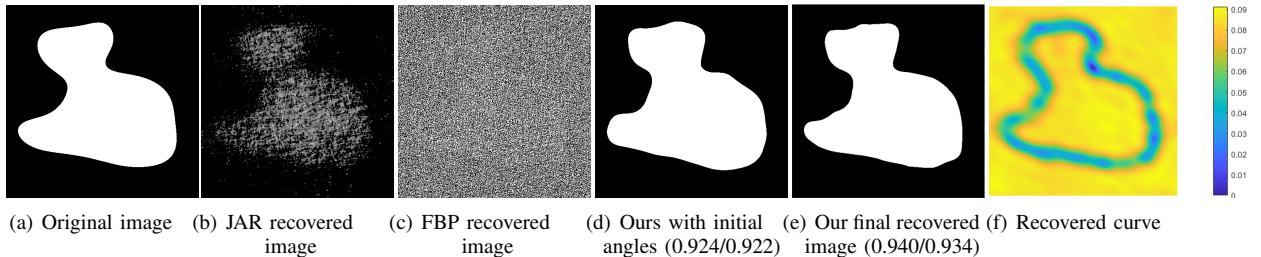


Fig. 5: Visual comparison of reconstructed images by our proposed method, JAR method and FBP method. Compared to the original image, the SSIM and IoU of our reconstructed image are 0.940 and 0.934 respectively (40 projection angles with  $\epsilon_\theta = 0.5$  rad, projection SNR = 5dB).

angles in the direction of the approximate gradient that reduce the cost function, and the angle step is gradually reduced until all the angles get updated once. We summarize the algorithm in **Algorithm 2**.

#### D. Scheme Overview

Based on the above process, the overall scheme is depicted in Fig. 2, which is consist of 1) Curve recovery given noisy projections and inaccurate initial angles using Eq. (5), 2) curve aware image recovery and 3) angle refinement based on the estimated 2D image.

## IV. EXPERIMENTAL RESULT

In order to estimate the performance of our proposed method, we consider curves with  $\rho(C) = (7, 7)$ . Projections

are taken at 40 angles and corrupted by noise so that the SNR of each projection is on average SNR = 5dB, as shown in Fig. 2. We assume the known angles deviate from the true values with  $\beta_i \sim U(-0.5, 0.5)$  rad. For Algorithm. 1, the choice of the regularization weights  $\lambda_1$  and  $\lambda_2$  balances the trade-off between encouraging piecewise smoothness of the image and preserving sharp edges. We set  $\lambda_1 = 5 \times 10^2$  and  $\lambda_2 = 0.5$  for the following experiments.<sup>1</sup> We use SSIM and IoU (Intersection over Union) to measure the reconstruction performance. For comparison, we also show the reconstruction results for filtered backprojection (FBP) method and the joint

<sup>1</sup>From our experiments, the choice of the tunable weights is not critical. A faithful reconstruction can be achieved with  $\lambda_1 \in [10^{-1}, 10^4]$  and  $\lambda_2 \in [10^{-3}, 10^1]$  (if the image range is [0,1]).

angular refinement (JAR) method proposed by Zehni *et. al* [17], as shown from Fig. 3 to Fig. 5. It is clear that due to the correct choice of the image model, the estimated polynomial is able to successfully yield the correct curve even with limited number of noisy projections and inaccurate initial angles. Apart from the robust FRI reconstruction algorithm, essential to the successful recovery of the curve is that we exploit the whole annihilating subspace, which makes the algorithm more robust under noisy scenarios. To be more specific, in the experiment we set  $\rho = (9, 9)$ . The FBP method fails due to heavy noise, while the JAR method can still recover the object despite blurring effect, due to model mismatch and lack of projections.

## V. CONCLUSIONS

In this work, we have proposed a robust algorithm for 2D tomographic reconstruction problem for 2D images defined by curves with finite rate of innovation. Unlike conventional methods that directly estimate the 2D objects, we instead leverage the frequency domain annihilation relation and retrieve the curve coefficients from noisy projections. Then the image is reconstructed based on a weighted total variation formulation of the spatial domain annihilation relation. Given the reconstructed image, we further refine the reconstruction by refining the estimation of the angles of the projections. The experiments have shown that after iterating this process twice, we get satisfactory reconstruction result even from severely noise corrupted projections and incorrect projection angles.

## REFERENCES

- [1] J. Frank, "Three-dimensional electron microscopy of macromolecular assemblies," in *Burlington: Academic Press*, 1996.
- [2] J. Drenth and J. R. Mesters, "Principles of protein X-ray crystallography," in *Springer New York*, 2007.
- [3] M. Van Heel, B. Gowen, R. Matadeen, E. V. Orlova, R. Finn, T. Pape, D. Cohen, H. Stark, R. Schmidt, and R. Schatz et al., "Single-particle electron cryo-microscopy: towards atomic resolution," in *Quarterly Reviews of Biophysics*, vol. 33, no. 4, pp. 307–369, 2000.
- [4] T. Bendory, A. Bartesaghi, and A. Singer, "Single- particle cryo-electron microscopy: Mathematical theory, computational challenges, and opportunities," in *IEEE Signal Processing Magazine*, vol. 37, no. 2, pp. 58–76, 2020.
- [5] S. H. Scheres, "RELION: Implementation of a bayesian approach to cryo-EM structure determination," in *Journal of Structural Biology*, vol. 180, no. 3, pp. 519–530, 2012.
- [6] R. Behling, "Modern diagnostic X-ray sources: Technology, manufacturing, reliability," in *CRC Press, Taylor Francis Group*, 2015.
- [7] DC. Lee, PF. Hoffmann, DL. Kopperdahl, TM. Keaveny, "Phantomless calibration of CT scans for measurement of BMD and bone strength-Inter-operator reanalysis precision", in *Bone*, 2017 Oct, 103:325-333.
- [8] S. Basu and Y. Bresler, "Uniqueness of tomography with unknown view angles," in *IEEE Transactions on Image Processing*, vol. 9, no. 6, pp. 1094–1106, 2000.
- [9] R. Wang, R. Alexandru and P. L. Dragotti, "Perfect Reconstruction of Classes of Non-Bandlimited Signals from Projections with Unknown Angles," in *IEEE International Conference on Acoustics, Speech and Signal Processing (ICASSP)*, Singapore 2022, pp. 5877-5881.
- [10] H. Stark, J. Woods, I. Paul and R. Hingorani, "Direct Fourier reconstruction in computer tomography," in *IEEE Transactions on Acoustics, Speech, and Signal Processing*, vol. 29, no. 2, pp. 237-245, April 1981.
- [11] A. H. Delaney and Y. Bresler, "A fast and accurate Fourier algorithm for iterative parallel-beam tomography," in *IEEE Transactions on Image Processing*, vol. 5, no. 5, pp. 740-753, May 1996.
- [12] EY. Sidky, X. Pan, "Image reconstruction in circular cone-beam computed tomography by constrained, total-variation minimization," in *Phys Med Biol*, 2008 Sep.
- [13] S. Niu, Y. Gao, Z. Bian, J. Huang, W. Chen, G. Yu, Z. Liang, J. Ma, "Sparse-view x-ray CT reconstruction via total generalized variation regularization", in *Phys Med Biol*, 2014 Jun 21;59(12):2997-3017.
- [14] H. Zhang, J. Wang, D. Zeng, X. Tao, J. Ma. "Regularization strategies in statistical image reconstruction of low-dose X-ray CT: A review", *Med Phys*, 2018 Oct;45(10):e886-e907.
- [15] C. Gong and L. Zeng, "Adaptive iterative reconstruction based on relative total variation for low-intensity computed tomography", in *Signal Process.*, vol. 165, pp. 149-162, 2019.
- [16] L. Donati, E. Soubies and M. Unser, "Inner-Loop-Free Admm For Cryo-Em," in *IEEE 16th International Symposium on Biomedical Imaging (ISBI 2019)*, pp. 307-311.
- [17] M. Zehni, L. Donati, E. Soubies, Z. Zhao and M. Unser, "Joint Angular Refinement and Reconstruction for Single-Particle Cryo-EM," in *IEEE Transactions on Image Processing*, vol. 29, pp. 6151-6163, 2020.
- [18] H. Pan, T. Blu and P. L. Dragotti, "Sampling Curves With Finite Rate of Innovation," in *IEEE Transactions on Signal Processing*, vol. 62, no. 2, pp. 458-471, Jan.15, 2014.
- [19] H. Pan, T. Blu and M. Vetterli, "Towards Generalized FRI Sampling With an Application to Source Resolution in Radioastronomy," in *IEEE Transactions on Signal Processing*, vol. 65, no. 4, pp. 821-835, 15 Feb.15, 2017.
- [20] M. Zhu, T. Chan, "An Efficient Primal-Dual Hybrid Gradient Algorithm For Total Variation Image Restoration", in *UCLA Cam Report*, Feb, 2005.